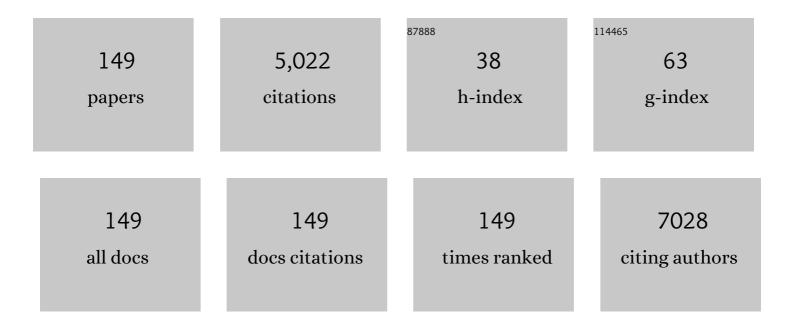
## Guangshe Li

List of Publications by Year in descending order

Source: https://exaly.com/author-pdf/1721522/publications.pdf Version: 2024-02-01



#	Article	IF	CITATIONS
1	Thermochemistry of nano-phased titanium dioxides relevant to energy application: A Review. Chemical Thermodynamics and Thermal Analysis, 2022, 5, 100033.	1.5	4
2	Layered Cu1–zMn1+zO2 Crednerite: Mapping the Phase Stabilization Region via Precise Compositional Control for Optimum Supercapacitor Performance. Inorganic Chemistry, 2022, 61, 2576-2586.	4.0	2
3	Fabrication of VO Nanorings on a Porous Carbon Architecture for High-Performance Li-Ion Batteries. ACS Applied Materials & Interfaces, 2022, 14, 9454-9463.	8.0	9
4	Low-Temperature Heat Capacities and Thermodynamic Functions of α-Bi2O3. Russian Journal of Physical Chemistry A, 2022, 96, 834-841.	0.6	0
5	Confinement chemistry of FeO <sub><i>x</i></sub> centers for activating molecular oxygen under ambient conditions. Nanoscale, 2022, 14, 9715-9723.	5.6	2
6	Chemically Homogenizing MoO <sub>2</sub> Nanocrystals into Monodispersed Spherical Shapes for Enhanced Cr(VI) Photoreduction. ACS Applied Nano Materials, 2022, 5, 9950-9957.	5.0	3
7	Control of dielectric properties in bismuth ferrite multiferroic by compacting pressure. Materials Chemistry and Physics, 2021, 258, 123925.	4.0	12
8	Migration of cations in layered oxides for creating a highly active interface toward CO preferential oxidation. Journal of Materials Chemistry A, 2021, 9, 12623-12635.	10.3	18
9	Growth kinetic control over MgFe <sub>2</sub> O <sub>4</sub> to tune Fe occupancy and metal–support interactions for optimum catalytic performance. CrystEngComm, 2021, 23, 2538-2546.	2.6	1
10	Zinc Ferrite Nanoparticles: Unusual Growth Mechanism for Sizeâ€Đependent Properties. ChemistrySelect, 2021, 6, 1862-1869.	1.5	6
11	Bonding the Terminal Isocyanate-Related Functional Group to the Surface Manganese Ions to Enhance Li-Rich Cathode's Cycling Stability. ACS Applied Materials & Interfaces, 2021, 13, 17565-17576.	8.0	17
12	Carbon coated Li3VO4 microsphere: Ultrafast solvothermal synthesis and excellent performance as lithium-ion battery anode. Journal of Power Sources, 2021, 493, 229680.	7.8	23
13	Size-encoded hierarchical self-assembly of nanoparticles into chains and tubules. Journal of Colloid and Interface Science, 2021, 604, 866-875.	9.4	1
14	Manipulating Surface Termination of Perovskite Manganate for Oxygen Activation. Advanced Functional Materials, 2021, 31, 2006439.	14.9	18
15	CsCu <sub>2</sub> 1 <sub>3</sub> Nanocrystals: Growth and Structural Evolution for Tunable Light Emission. ACS Omega, 2021, 6, 544-552.	3.5	26
16	Understanding the Doping Chemistry of High Oxidation States in Scheelite CaWO4 by Hydrothermal Conditions. Inorganic Chemistry, 2021, 60, 16558-16569.	4.0	2
17	Site occupancy and tunable photoluminescence properties of Eu2+-Activated Ba3Sc(BO3)3 phosphors for white light emitting diodes. Journal of Alloys and Compounds, 2020, 815, 152645.	5.5	23
18	A novel core–double shell heterostructure derived from a metal–organic framework for efficient HER, OER and ORR electrocatalysis. Inorganic Chemistry Frontiers, 2020, 7, 191-197.	6.0	45

#	Article	IF	CITATIONS
19	Evidence for the influence of polaron delocalization on the electrical transport in LiNi <sub>0.4+x</sub> Mn <sub>0.4â^*x</sub> 0.2O <sub>2</sub> . Physical Chemistry Chemical Physics, 2020, 22, 2054-2060.	2.8	6
20	Role of double interfaces in inspiring energy storage devices in CC@Ni(OH)Cl@NiO flexible electrodes. Materials Chemistry Frontiers, 2020, 4, 231-242.	5.9	5
21	A survey of current trends in computational predictions of protein-protein interactions. Frontiers of Computer Science, 2020, 14, 1.	2.4	19
22	Layer-by-layer assembly into bulk-like g-C3N4via artificial manipulation of electrostatic forces. Chemical Communications, 2020, 56, 15663-15666.	4.1	7
23	In Situ Growth of Amorphous NiFe Hydroxides on Spinel NiFe <sub>2</sub> O <sub>4</sub> via Ultrasonic-Assisted Reduction for an Enhanced Oxygen Evolution Reaction. ACS Sustainable Chemistry and Engineering, 2020, 8, 17194-17200.	6.7	23
24	Photocatalytic Hydrogen Evolution Performance for Hydroxyl-rich Porous Carbon Nitride. Chemical Research in Chinese Universities, 2020, 36, 1053-1058.	2.6	4
25	Pressureâ€Driven Eu <sup>2+</sup> â€Doped BaLi <sub>2</sub> Al <sub>2</sub> Si <sub>2</sub> N <sub>6</sub> : A New Color Tunable Narrowâ€Band Emission Phosphor for Spectroscopy and Pressure Sensor Applications. Advanced Functional Materials. 2020. 30. 2001384.	14.9	63
26	F doped Li3VO4: An advanced anode material with optimized rate capability and durable lifetime. Electrochimica Acta, 2020, 354, 136655.	5.2	14
27	Topological transformation of LDH nanosheets to highly dispersed PtNiFe nanoalloys enhancing CO oxidation performance. Nanoscale, 2020, 12, 14882-14894.	5.6	18
28	Tetracycline Removal Under Solar Illumination Over Ag <sub>3</sub> VO <sub>4</sub> /mpgâ€C <sub>3</sub> N <sub>4</sub> Heterojunction Photocatalysts. Photochemistry and Photobiology, 2019, 95, 501-511.	2.5	12
29	A symbiotic hetero-nanocomposite that stabilizes unprecedented CaCl <sub>2</sub> -type TiO <sub>2</sub> for enhanced solar-driven hydrogen evolution reaction. Chemical Science, 2019, 10, 8323-8330.	7.4	14
30	Synthesis of CeO2 assemblies through interaction with short-chain dicarboxylic acids under facile hydrothermal conditions. RSC Advances, 2019, 9, 28581-28587.	3.6	3
31	Atomicâ€Scale Insights into Surface Lattice Oxygen Activation at the Spinel/Perovskite interface of Co <sub>3</sub> O <sub>4</sub> /La <sub>0.3</sub> Sr <sub>0.7</sub> CoO <sub>3</sub> . Angewandte Chemie - International Edition, 2019, 58, 11720-11725.	13.8	140
32	Atomic‣cale Insights into Surface Lattice Oxygen Activation at the Spinel/Perovskite interface of Co 3 O 4 /La 0.3 Sr 0.7 CoO 3. Angewandte Chemie, 2019, 131, 11846-11851.	2.0	26
33	Unveiling the Impact of the Polypyrrole Coating Layer Thickness on the Electrochemical Performances of LiNi <sub>0.5</sub> Co <sub>0.2</sub> Mn <sub>0.3</sub> O <sub>2</sub> in Li–lon Battery. ChemistrySelect, 2019, 4, 6354-6360.	1.5	20
34	Optimizing giant dielectric properties via interface composition: A study of rutile-based ceramics. Ceramics International, 2019, 45, 17705-17714.	4.8	5
35	Reconstructing the Surface Structure of Li-Rich Cathodes for High-Energy Lithium-Ion Batteries. ACS Applied Materials & Interfaces, 2019, 11, 19950-19958.	8.0	37
36	Heat capacity and thermodynamic functions of hollandite-type K0.17TiO1.9·0.061H2O. Journal of Chemical Thermodynamics, 2019, 137, 34-42.	2.0	3

#	Article	IF	CITATIONS
37	lron-Doped LiCoO2 Nanosheets as Highly Efficient Electrocatalysts for Alkaline Water Oxidation. European Journal of Inorganic Chemistry, 2019, 2019, 2448-2454.	2.0	6
38	Temperatureâ€dependent electrical transport behavior and structural evolution in hollanditeâ€ŧype titaniumâ€based oxide. Journal of the American Ceramic Society, 2019, 102, 6741-6750.	3.8	7
39	Facile synthesis of Mn2.1V0.9O4/rGO: A novel high-rate anode material for lithium-ion batteries. Journal of Power Sources, 2019, 426, 197-204.	7.8	28
40	Black Phosphorus-Modified Co <sub>3</sub> O <sub>4</sub> through Tuning the Electronic Structure for Enhanced Oxygen Evolution Reaction. ACS Applied Materials & Interfaces, 2019, 11, 17459-17466.	8.0	87
41	A facile strategy to fabricate V2O3/Porous N-doped carbon nanosheet framework as high-performance anode for lithium-ion batteries. Journal of Alloys and Compounds, 2019, 789, 288-294.	5.5	28
42	Remarkable Improvement in Photocatalytic Performance for Tannery Wastewater Processing via SnS <sub>2</sub> Modified with Nâ€Doped Carbon Quantum Dots: Synthesis, Characterization, and 4â€Nitrophenolâ€Aided Cr(VI) Photoreduction. Small, 2019, 15, e1804515.	10.0	44
43	Effect of Alloyed BiOCl <sub>x</sub> Br <sub>1â€x</sub> Nanosheets Thickness on the Photocatalytic Performance. ChemistrySelect, 2019, 4, 1757-1762.	1.5	8
44	Kinetic control of CeO2 nanoparticles for catalytic CO oxidation. Journal of Materials Research, 2019, 34, 2201-2208.	2.6	9
45	A LiPF <sub>6</sub> -electrolyte-solvothermal route for the synthesis of LiF/Li <sub>x</sub> PF <sub>y</sub> O <sub>z</sub> -coated Li-rich cathode materials with enhanced cycling stability. Journal of Materials Chemistry A, 2019, 7, 23149-23161.	10.3	37
46	Partial surface phase transformation of Li3VO4 that enables superior rate performance and fast lithium-ion storage. Tungsten, 2019, 1, 276-286.	4.8	22
47	Strongly Coupled Amorphous Porous NbO x (OH) y /g  3 N 4 Heterostructure Composite for Efficient Photocatalytic Hydrogen Evolution. ChemistrySelect, 2019, 4, 13506-13516.	1.5	2
48	Tunable photoluminescence properties and energy transfer of Ca5(BO3)3F: Tb3+/Eu3+ phosphors for solid state lighting. Journal of Luminescence, 2019, 208, 155-163.	3.1	19
49	Heatâ€Treatmentâ€Assisted Moltenâ€Salt Strategy to Enhance Electrochemical Performances of Liâ€Rich Assembled Microspheres by Tailoring Their Surface Features. Chemistry - A European Journal, 2019, 25, 2003-2010.	3.3	10
50	An insight into the polarization mechanism of rutile based oxides with a wide doping levels in the TiO2-CuO-TaO2.5 ternary system. Journal of Alloys and Compounds, 2019, 780, 8-16.	5.5	6
51	Co <sub>3</sub> O <sub>4</sub> –CuCoO <sub>2</sub> Nanomesh: An Interface-Enhanced Substrate that Simultaneously Promotes CO Adsorption and O <sub>2</sub> Activation in H <sub>2</sub> Purification. ACS Applied Materials & Interfaces, 2019, 11, 6042-6053.	8.0	55
52	TaCxOy: A photocatalytic promoter on g-C3N4 for visible-light Cr6+ reduction. Catalysis Communications, 2019, 119, 129-133.	3.3	16
53	Crystalline/amorphous Al/Al2O3 core/shell nanospheres as efficient catalysts for the selective transfer hydrogenation of α,β-unsaturated aldehydes. Catalysis Communications, 2018, 109, 50-54.	3.3	9
54	Facile synthesis of Fe4N/Fe2O3/Fe/porous N-doped carbon nanosheet as high-performance anode for lithium-ion batteries. Journal of Power Sources, 2018, 384, 34-41.	7.8	51

#	Article	IF	CITATIONS
55	Tunable green/red dual-mode luminescence via energy management in core-multishell nanoparticles. Materials and Design, 2018, 152, 119-128.	7.0	14
56	In Situ Growth of MoS <sub>2</sub> Nanosheet Arrays and TS <sub>2</sub> (T = Fe, Co, and Ni) Nanocubes onto Molybdate for Efficient Oxygen Evolution Reaction and Improved Hydrogen Evolution Reaction. ACS Omega, 2018, 3, 464-471.	3.5	20
57	Optimum Preferential Oxidation Performance of CeO <sub>2</sub> –CuO <sub><i>x</i></sub> –RGO Composites through Interfacial Regulation. ACS Applied Materials & Interfaces, 2018, 10, 7935-7945.	8.0	55
58	Amorphous tantalum oxyhydroxide homojunction: In situ construction for enhanced hydrogen production. Journal of Colloid and Interface Science, 2018, 525, 196-205.	9.4	17
59	In Situ Synthesis of Mn <sub>3</sub> O <sub>4</sub> Nanoparticles on Hollow Carbon Nanofiber as Highâ€Performance Lithiumâ€Ion Battery Anode. Chemistry - A European Journal, 2018, 24, 9632-9638.	3.3	37
60	Anion De/Intercalation in Nickel Hydroxychloride Microspheres: A Mechanistic Study of Structural Impact on Energy Storage Performance of Multianion-Containing Layered Materials. ACS Applied Energy Materials, 2018, 1, 1522-1533.	5.1	14
61	Unprecedented catalytic performance in amine syntheses <i>via</i> Pd/g-C <sub>3</sub> N <sub>4</sub> catalyst-assisted transfer hydrogenation. Green Chemistry, 2018, 20, 2038-2046.	9.0	91
62	Organic titanates: a model for activating rapid room-temperature synthesis of shape-controlled CsPbBr <sub>3</sub> nanocrystals and their derivatives. Chemical Communications, 2018, 54, 3863-3866.	4.1	17
63	Highly Luminescent CsPbX <sub>3</sub> (X=Cl, Br, I) Nanocrystals Achieved by a Rapid Anion Exchange at Room Temperature. Chemistry - A European Journal, 2018, 24, 1898-1904.	3.3	25
64	Predicting Protein Interactions Using a Deep Learning Method-Stacked Sparse Autoencoder Combined with a Probabilistic Classification Vector Machine. Complexity, 2018, 2018, 1-12.	1.6	17
65	Morphology engineering of nickel molybdate hydrate nanoarray for electrocatalytic overall water splitting: from nanorod to nanosheet. RSC Advances, 2018, 8, 35131-35138.	3.6	25
66	In situ synthesis of V <sub>2</sub> O <sub>3</sub> nanorods anchored on reduced graphene oxide as highâ€performance lithium ion battery anode. ChemistrySelect, 2018, 3, 12108-12112.	1.5	13
67	Simply Constructing Li <sub>1.2</sub> Mn <sub>0.6</sub> Ni <sub>0.2</sub> O <sub>2</sub> /C Composites for Superior Electrochemical Performance and Thermal Stability in Li–Ion Battery. ChemistrySelect, 2018, 3, 13647-13653.	1.5	3
68	Architecture of Biomimetic Water Oxidation Catalyst with Mn <sub>4</sub> CaO <sub>5</sub> Clusterlike Structure Unit. ACS Applied Materials & Interfaces, 2018, 10, 37948-37954.	8.0	14
69	Crystal Growth of Bimetallic Oxides CuMnO <sub>2</sub> with Tailored Valence States for Optimum Electrochemical Energy Storage. Crystal Growth and Design, 2018, 18, 6107-6116.	3.0	28
70	Preferential Neighboring Substitution-Triggered Full Visible Spectrum Emission in Single-Phased Ca <sub>10.5–<i>x</i></sub> Mg <i><sub>x</sub></i> (PO <sub>4</sub> ) <sub>7</sub> :Eu <sup>2+</sup> Phosphors for High Color-Rendering White LEDs. ACS Applied Materials & Interfaces, 2018, 10, 33322-33334.	8.0	84
71	Stabilizing Co 4+ Ions in Ultrathin Cobalt Oxide Nanosheets for Efficient Oxygen Evolution Reaction. ChemCatChem, 2018, 10, 4888-4893.	3.7	6
72	Surface hydroxylation induced by alkaline-earth metal doping in NiO nanocrystals and its application in achieving a wide temperature operation window for preferential CO oxidation. Environmental Science: Nano, 2018, 5, 2368-2381.	4.3	18

#	Article	IF	CITATIONS
73	Fe3+ doped amorphous Co2BOy(OH)z with enhanced activity for oxygen evolution reaction. Electrochimica Acta, 2018, 280, 1-8.	5.2	28
74	Activation of Surface Oxygen Sites in a Cobalt-Based Perovskite Model Catalyst for CO Oxidation. Journal of Physical Chemistry Letters, 2018, 9, 4146-4154.	4.6	67
75	Interfacial Doping of Heteroatom in Porous SnO <sub>2</sub> for Highly Sensitive Surface Properties. ACS Omega, 2018, 3, 6988-6997.	3.5	8
76	CdO-CuO-TiO2 ternary dielectric systems: Subsolidus phase diagram and the effects of Cu segregation. Journal of the European Ceramic Society, 2018, 38, 4978-4985.	5.7	22
77	Phosphotungstic acid binding in situ to K4Nb6O17 for the effective adsorption-photocatalytic removal of tetracycline. Journal of Nanoparticle Research, 2018, 20, 1.	1.9	12
78	Fast synthesis of Co <sub>1.8</sub> V <sub>1.2</sub> O <sub>4</sub> /rGO as a high-rate anode material for lithium-ion batteries. Chemical Communications, 2018, 54, 7689-7692.	4.1	24
79	A high-yield and versatile method for the synthesis of carbon dots for bioimaging applications. Journal of Materials Chemistry B, 2017, 5, 1935-1942.	5.8	42
80	Ultrathin LiCoO <sub>2</sub> Nanosheets: An Efficient Water-Oxidation Catalyst. ACS Applied Materials & Interfaces, 2017, 9, 7100-7107.	8.0	47
81	A bridge role of Tb3+ in broadband excited Sr3Y(PO4)3:Ce3+, Tb3+, Sm3+ phosphors with superior thermal stability. Materials and Design, 2017, 118, 245-255.	7.0	37
82	Kinetic Control of Hexagonal Mg( <scp>OH</scp> ) <sub>2</sub> Nanoflakes for Catalytic Application of Preferential <scp>CO</scp> Oxidation. Chinese Journal of Chemistry, 2017, 35, 903-910.	4.9	5
83	Pristine Surface Investigation of Li1.2Mn0.54Ni0.13Co0.13O2 towards Improving Capacity and Rate-capability for Lithium-ion Batteries. Electrochimica Acta, 2017, 245, 118-127.	5.2	9
84	Synthesis of a Ternary Thiostannate with 3D Channel Decorated by Hydronium for High Proton Conductivity. Inorganic Chemistry, 2017, 56, 208-212.	4.0	15
85	Growth Kinetics, Cation Occupancy, and Magnetic Properties of Multimetal Oxide Nanoparticles: A Case Study on Spinel NiFe <sub>2</sub> O <sub>4</sub> . Journal of Physical Chemistry C, 2017, 121, 19467-19477.	3.1	36
86	Nanosized amorphous tantalum oxide: a highly efficient photocatalyst for hydrogen evolution. Research on Chemical Intermediates, 2017, 43, 5011-5024.	2.7	22
87	Crystalline-to-amorphous transformation of tantalum-containing oxides for a superior performance in unassisted photocatalytic water splitting. International Journal of Hydrogen Energy, 2017, 42, 21006-21015.	7.1	10
88	In situ synthesis of NIR-light emitting carbon dots derived from spinach for bio-imaging applications. Journal of Materials Chemistry B, 2017, 5, 7328-7334.	5.8	93
89	Tuning shell thickness of MnO/C core-shell nanowires for optimum performance of lithium-ion batteries. Chemical Research in Chinese Universities, 2017, 33, 924-928.	2.6	8
90	Frontispiece: Smart Solution Chemistry to Sn ontaining Intermetallic Compounds through a Selfâ€Disproportionation Process. Chemistry - A European Journal, 2016, 22, .	3.3	0

#	Article	IF	CITATIONS
91	Exploration of spin state and exchange integral of cobalt ions in stoichiometric ZnCo2O4 spinel oxides. Applied Physics Letters, 2016, 108, .	3.3	14
92	Advances of solution chemistry in stabilizing different crystal phases of inorganic nano-compounds. CrystEngComm, 2016, 18, 9209-9222.	2.6	12
93	δ-MnO <sub>2</sub> –Mn <sub>3</sub> O <sub>4</sub> Nanocomposite for Photochemical Water Oxidation: Active Structure Stabilized in the Interface. ACS Applied Materials & Interfaces, 2016, 8, 27825-27831.	8.0	60
94	Electron competitive migration regulating for dual maxima of water photolysis. RSC Advances, 2016, 6, 995-1003.	3.6	18
95	Fabrication of Li-Rich Cathodes with Enhanced Stability and Electrochemical Performances for Lithium Ion Battery. ECS Meeting Abstracts, 2016, , .	0.0	0
96	LiMO2 (MÂ=ÂMn, Co, Ni) hexagonal sheets with (101) facets for ultrafast charging–discharging lithium ion batteries. Journal of Power Sources, 2015, 276, 238-246.	7.8	20
97	Coupled Heterojunction Sn <sub>2</sub> Ta <sub>2</sub> O <sub>7</sub> @SnO <sub>2</sub> : Cooperative Promotion of Effective Electron–Hole Separation and Superior Visible-light Absorption. ACS Applied Materials & Interfaces, 2015, 7, 13905-13914.	8.0	22
98	Hydrothermal-Assisted Synthesis of Li-Rich Layered Oxide Microspheres with High Capacity and Superior Rate-capability as a Cathode for Lithium-ion Batteries. Electrochimica Acta, 2015, 173, 7-16.	5.2	62
99	Anchoring High-Concentration Oxygen Vacancies at Interfaces of CeO <sub>2–<i>x</i></sub> /Cu toward Enhanced Activity for Preferential CO Oxidation. ACS Applied Materials & Interfaces, 2015, 7, 22999-23007.	8.0	173
100	Eu3+-doped Y2O3 hexagonal prisms: Shape-controlled synthesis and tailored luminescence properties. Journal of Alloys and Compounds, 2015, 647, 648-659.	5.5	18
101	A Study on Storage Characteristics of Pristine Li-rich Layered Oxide Li 1.20 Mn 0.54 Co 0.13 Ni 0.13 O 2 : Effect of Storage Temperature and Duration. Electrochimica Acta, 2015, 154, 249-258.	5.2	30
102	Graphene nanoribbons generate a strong third-order nonlinear optical response upon intercalating hexagonal boron nitride. Journal of Materials Chemistry C, 2014, 2, 1482.	5.5	47
103	Ce0.9Fe0.1O1.97/Ag: a cheaper inverse catalyst with excellent oxygen storage capacity and improved activity towards CO oxidation. Catalysis Science and Technology, 2014, 4, 402-410.	4.1	15
104	Hybridization of brookite TiO <sub>2</sub> with g-C <sub>3</sub> N <sub>4</sub> : a visible-light-driven photocatalyst for As <sup>3+</sup> oxidation, MO degradation and water splitting for hydrogen evolution. Journal of Materials Chemistry A, 2014, 2, 15774-15780.	10.3	117
105	Heterosturcture NiO/Ce1â^'xNixO2: synthesis and synergistic effect of simultaneous surface modification and internal doping for superior catalytic performance. RSC Advances, 2014, 4, 6397.	3.6	24
106	Searching for cheaper catalysts with high activity and stability in Ce–M–O systems (M = Fe, Co, Ni). Catalysis Science and Technology, 2014, 4, 3368-3378.	4.1	15
107	Enhancement of thermal stability in bismuth phosphate by Ln3+ doping for tailored luminescence properties. CrystEngComm, 2014, 16, 5040.	2.6	10
108	Atomic-scale control of TiO6 octahedra through solution chemistry towards giant dielectric response. Scientific Reports, 2014, 4, 6582.	3.3	62

#	Article	IF	CITATIONS
109	Facile synthesis of composite g-C3N4/WO3: a nontoxic photocatalyst with excellent catalytic activity under visible light. RSC Advances, 2013, 3, 13646.	3.6	95
110	Lattice defect quenching effects on luminescence properties of Eu3+-doped YVO4 nanoparticles. Journal of Nanoparticle Research, 2013, 15, 1.	1.9	8
111	An ultra-stable nanosized Ce <sub>0.9</sub> Fe <sub>0.1</sub> O <sub>2</sub> solid solution with an excellent catalytic performance towards CH <sub>4</sub> oxidation. Journal of Materials Chemistry A, 2013, 1, 374-380.	10.3	30
112	Direct synthesis of carbon-coated Li4Ti5O12 mesoporous nanoparticles for high-rate lithium-ion batteries. RSC Advances, 2013, 3, 3088.	3.6	19
113	Exploring the unique electrical properties of metastable BiPO <sub>4</sub> through switchable phase transitions. CrystEngComm, 2013, 15, 609-615.	2.6	27
114	Intrinsic Reason for the Morphology Dependence of Luminescent Behavior: A Case Study with GdVO <sub>4</sub> :Eu <sup>3+</sup> Nanocrystals. European Journal of Inorganic Chemistry, 2013, 2013, 5999-6008.	2.0	7
115	Enhancing Photocatalytic Performance through Tuning the Interfacial Process between -Assembled and Pt-Loaded Microspheres. International Journal of Photoenergy, 2012, 2012, 1-7.	2.5	2
116	Spin state transition and giant dielectric constant in Pr0.987Na0.013CoO3. Applied Physics Letters, 2012, 100, 152109.	3.3	6
117	One-step synthesis of SbPO4 hollow spheres by a self-sacrificed template method. RSC Advances, 2012, 2, 12999.	3.6	7
118	Low-concentration donor-doped LiCoO2 as a high performance cathode material for Li-ion batteries to operate between â^'10.4 and 45.4 °C. Journal of Materials Chemistry, 2012, 22, 22233.	6.7	76
119	Fabrication of assembled-spheres YVO4:(Ln3+, Bi3+) towards optically tunable emission. CrystEngComm, 2012, 14, 2062.	2.6	44
120	Solvent-driven polymorphic control of CdWO4 nanocrystals for photocatalytic performances. New Journal of Chemistry, 2012, 36, 1852.	2.8	24
121	pH-driven hydrothermal synthesis and formation mechanism of all BiPO4 polymorphs. CrystEngComm, 2012, 14, 7907.	2.6	33
122	Synthesis of High-Quality Brookite TiO <sub>2</sub> Single-Crystalline Nanosheets with Specific Facets Exposed: Tuning Catalysts from Inert to Highly Reactive. Journal of the American Chemical Society, 2012, 134, 8328-8331.	13.7	251
123	Fabrication of Ag–CeO2 core–shell nanospheres with enhanced catalytic performance due to strengthening of the interfacial interactions. Journal of Materials Chemistry, 2012, 22, 10480.	6.7	98
124	A novel approach to composite electrode 0.3Li2MnO3–0.7LiMn1/3Ni1/3Co1/3O2 in lithium-ion batteries with an anomalous capacity and cycling stability at 45.4 °C. Scripta Materialia, 2012, 66, 300-303.	5.2	33
125	MgAl2O4 nanoparticles: A new low-density additive for accelerating thermal decomposition of ammonium perchlorate. RSC Advances, 2011, 1, 1808.	3.6	26
126	Uncovering the structural stabilities of the functional bismuth containing oxides: a case study of α-Bi <sub>2</sub> O <sub>3</sub> nanoparticles in aqueous solutions. New Journal of Chemistry, 2011, 35, 197-203.	2.8	17

#	Article	IF	CITATIONS
127	Preparation and polymorph-sensitive luminescence properties of BiPO4:Eu, Part I: room-temperature reaction followed by a heat treatment. CrystEngComm, 2011, 13, 6251.	2.6	78
128	Solvothermal synthesis of hierarchical SnIn4S8 microspheres and their application in photocatalysis. Research on Chemical Intermediates, 2011, 37, 297-307.	2.7	10
129	Understanding the defect chemistry of oxide nanoparticles for creating new functionalities: A critical review. Science China Chemistry, 2011, 54, 876-886.	8.2	18
130	Control Over the Crystallinity and Defect Chemistry of YVO <sub>4</sub> Nanocrystals for Optimum Photocatalytic Property. European Journal of Inorganic Chemistry, 2011, 2011, 2211-2220.	2.0	61
131	Magnetism of Zn0.75Cr0.25S with ordered doping configurations predicted by generalized gradient approximation plus Hubbard U. Journal of Applied Physics, 2011, 109, 083925.	2.5	1
132	Dynamics of Water Confined on the Surface of Titania and Cassiterite Nanoparticles. Materials Research Society Symposia Proceedings, 2011, 1352, 47.	0.1	3
133	Supersaturated spontaneous nucleation to TiO2 microspheres: synthesis and giant dielectric performance. Chemical Communications, 2010, 46, 3113.	4.1	28
134	Tailoring the nanoscale boundary cavities in rutile TiO2 hierarchical microspheres for giant dielectric performance. Journal of Materials Chemistry, 2010, 20, 8659.	6.7	36
135	Chemical modifications of red phosphor LaPO <sub>4</sub> :Eu3+nanorods to generate white light. Journal of Materials Chemistry, 2010, 20, 459-465.	6.7	61
136	Preparation of cereal-like Y V O <sub>4</sub> :Ln <sup>3 +</sup> (Ln = Sm, Eu, Tb, Dy) for high quantum efficiency photoluminescence. Nanotechnology, 2010, 21, 195601.	2.6	66
137	Insights into the roles of organic coating in tuning the defect chemistry of monodisperse TiO2 nanocrystals for tailored properties. Physical Chemistry Chemical Physics, 2010, 12, 10857.	2.8	31
138	Surface doping for photocatalytic purposes: relations between particle size, surface modifications, and photoactivity of SnO <sub>2</sub> :Zn <sup>2+</sup> nanocrystals. Nanotechnology, 2009, 20, 155706.	2.6	67
139	Generation of tunable wavelength lights in core-shell CaWO4 microspheres via co-doping with Na+ and Ln3+ (Ln = Tb, Sm, Dy, Eu). Journal of Materials Chemistry, 2009, 19, 2316.	6.7	58
140	Nature of Catalytic Activities of CoO Nanocrystals in Thermal Decomposition of Ammonium Perchlorate. Inorganic Chemistry, 2008, 47, 8839-8846.	4.0	112
141	Origin of the Enhanced Photocatalytic Activities of Semiconductors: A Case Study of ZnO Doped with Mg <sup>2+</sup> . Journal of Physical Chemistry C, 2008, 112, 12242-12248.	3.1	229
142	Synthesis and Optimum Luminescence of CaWO <sub>4</sub> -Based Red Phosphors with Codoping of Eu <sup>3+</sup> and Na <sup>+</sup> . Chemistry of Materials, 2008, 20, 6060-6067.	6.7	317
143	Inheriting morphology and photoluminescence properties of MgO nanoplates. Journal of Materials Research, 2007, 22, 908-912.	2.6	12
144	Nature of the abnormal band gap narrowing in highly crystalline Zn1â^'xCoxO nanorods. Applied Physics Letters, 2006, 88, 114103.	3.3	56

#	Article	IF	CITATIONS
145	Correlation between size-induced lattice variations and yellow emission shift in ZnO nanostructures. Applied Physics Letters, 2005, 87, 124101.	3.3	42

Hydrothermal synthesis and characterization of nanocrystalline pyrochlore oxides M2Sn2O7 (M = La,) Tj ETQq0 0 0 rgBT /Overlock 10 To 0.7 gPT /O

147	Valence Characteristics and Structural Stabilities of the Electrolyte Solid Solutions Ce1-xRExO2- $\hat{I}'$ (RE) Tj ETQq1 1	0.784314	rggT /Overle
148	Solid Solubility and Transport Properties of Nanocrystalline(CeO2)1-x(BiO1.5)xby Hydrothermal Conditions. Chemistry of Materials, 1999, 11, 1259-1266.	6.7	57
149	The study of <sup>57</sup> Fe Mössbauer spectra for La <sub>0.7</sub> Sr <sub>0.3</sub> FeO <sub>3â^Î</sub> with different structure. Physica Status Solidi (B): Basic Research, 1996, 197, 165-172.	1.5	3